PCCP

ROYAL SOCIETY OF CHEMISTRY

PAPER

View Article Online
View Journal | View Issue

Cite this: *Phys. Chem. Chem. Phys.*, 2023, **25**, 16781

Rationalizing the formation of porosity in mechanochemically-synthesized polymers†

Annika Krusenbaum, Steffi Krause Hinojosa, Sven Fabig, Valentin Becker, Sven Grätz and Lars Borchardt *

Received 9th May 2023,
Accepted 8th June 2023

DOI: 10.1039/d3cp02128a

rsc.li/pccp

In this study, we present a matrix of 144 mechanochemically-synthesized polymers. All polymers were constructed by the solvent-free Friedel–Crafts polymerization approach, employing 16 aryl-containing monomers and 9 halide-containing linkers, which were processed in a high-speed ball mill. This Polymer Matrix was utilized to investigate the origin of porosity in Friedel–Crafts polymerizations in detail. By examining the physical state, molecular size, geometry, flexibility, and electronic structure of the utilized monomers and linkers, we identified the most important factors influencing the formation of porous polymers. We analyzed the significance of these factors for both monomers and linkers based on the yield and specific surface area of the generated polymers. Our in-depth evaluation serves as a benchmark study for future targeted design of porous polymers by the facile and sustainable concept of mechanochemistry.

Introduction

The increasing relevance of porous polymers, which is attributed to their application in molecular separations, in gas and energy storage, or in catalysis, resulted in an ever-growing interest in these materials over recent decades.[1–16] Porous organic polymers (POPs) in particular have recently moved into the scientific and industrial focus, attributed to their unique combination of large and accessible surface areas with significant chemical and thermal stabilities.[17–20] The broad range of possible molecular building blocks linked by covalent bonds also leads to a high diversity of these lightweight and structurally flexible polymers.[21–25]

Despite their increasing value, the syntheses of POPs often face significant drawbacks. Classical solution-based protocols typically require expensive starting materials or catalysts.[26,27] Furthermore, these polymers tend to have a modest degree of polymerization, as the products can precipitate rapidly. Additionally, the solvents used in these protocols are a major source of waste generation in the chemical industry today.[28–30]

The drawbacks of solution-based protocols have created a demand for alternative reaction pathways, with mechanochemistry arising as one of the top 10 emerging innovations in chemistry, according to the International Union of Pure and Applied Chemistry (IUPAC).[31] Unlike solution-based protocols, mechanochemical reactions are initiated by mechanical force, resulting in a solvent-free and straightforward reaction, attributed to a constant generation of reactive surface and adequate mass transportation.[32] Mechanochemistry offers several advantages over traditional solution-based protocols, including circumventing the production of toxic solvent waste and faster reaction rates.[33–37]

Due to the numerous advantages it offers, the mechanochemical generation of POPs has received increasing attention in recent years.[32,38–41] Lewis acid-catalyzed polycondensation protocols, such as the Scholl or Friedel–Crafts polymerization, are particularly popular due to their speed, versatility, and cost efficiency.[42–48] During these reactions, a significant amount of HCl is released into the sealed milling vessels, which has a direct impact on the porosity of the generated polymers.[42] Additionally, the setup of milling parameters and choice of liquid-assisted grinding agents have also been found to be crucial in this regard.[44,47] Despite these developments, ball mills are still considered as ''black boxes'', and a deep understanding of the underlying principles that result in the formation of porous polymers is urgently required.

To address the need for a better understanding of mechanochemical synthesis and its impact on the formation of porous polymers, we present a matrix of mechanochemically-synthesized polymers based on a Friedel–Crafts reaction. By using a sophisticated variation of structurally diverse monomers and linkers, we aim to elucidate the impact of the molecular design of the building blocks on the mechanochemical formation of porous polymers (Fig. 1). This study is intended to simplify the prediction of the porosity of a desired

Inorganic Chemistry I, Ruhr-Universität Bochum, Universitätsstraße 150, 44801 Bochum, Germany. E-mail: lars.borchardt@rub.de

† Electronic supplementary information (ESI) available. See DOI: https://doi.org/10.1039/d3cp02128a

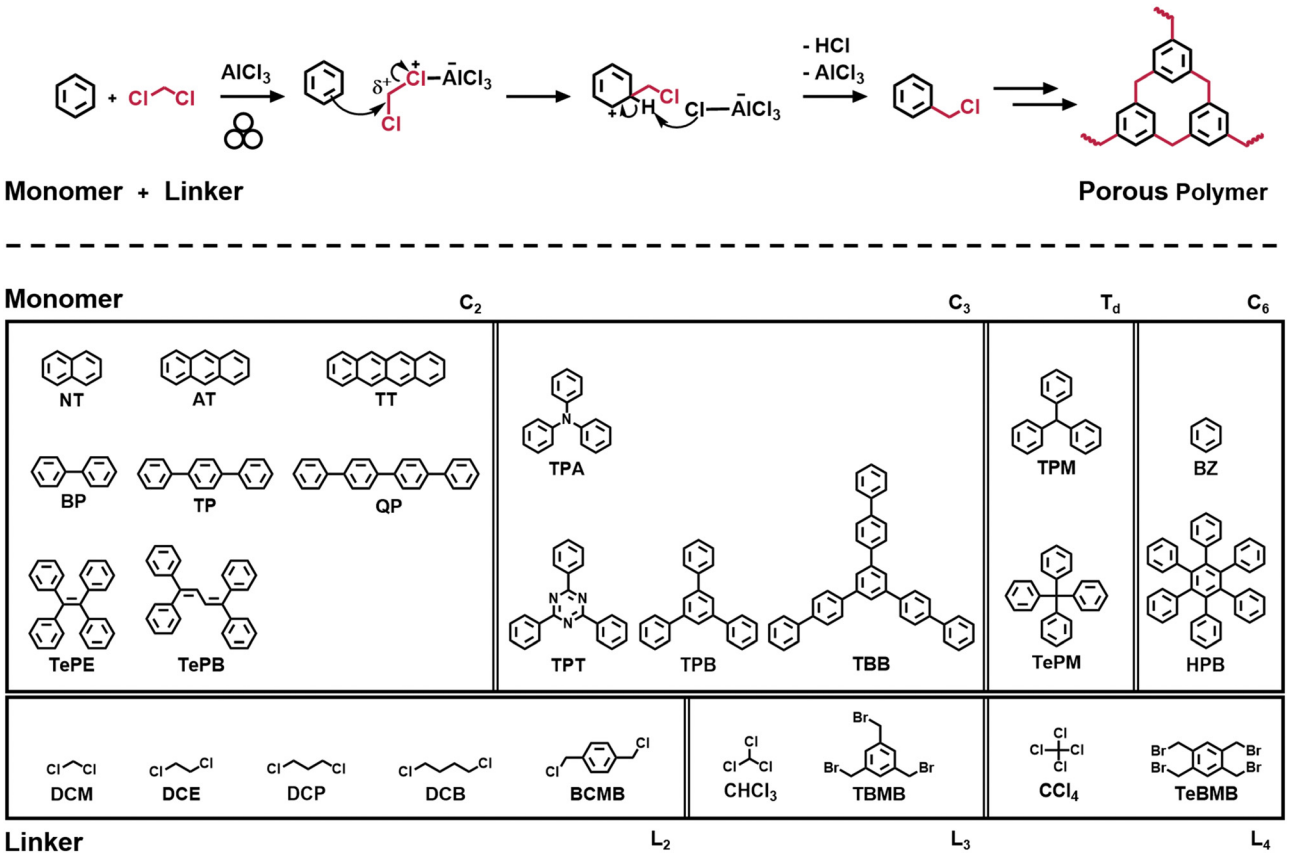

Fig. 1 Top: Schematic overview over the mechanochemical Friedel–Crafts polymerization of a monomer and linker towards a porous polymer on the example of benzene and dichloromethane, catalysed by the Lewis acid $AlCl_3$. The coordination of $AlCl_3$ and the linker leads to a positive polarization at the adjacent carbon that can be attacked by the high electron density of the monomer and form a polymer under release of HCl and rearomatisation. Bottom: Overview over monomers and linkers used in the Polymer Matrix. The monomers are sorted with respect to their symmetric unit: C_2: Naphthalene (NT), Anthracene (AT), Tetracene (TT), Biphenyl (BP), *p*-Terphenyl (TP), *p*-Quaterphenyl (QT), Tetraphenylethylene (TePE), and Tetraphenylbutadiene (TePB); C_3: Triphenylamine (TPA), Triphenyltriazine (TPT), Triphenylbenzene (TPB), and Tris(*p*-biphenyl)benzene (TBB); T_d: Triphenylmethane (TPM) and Tetraphenylmethane (TePM); C_6: Benzene (BZ) and Hexaphenylbenzene (HPB). The linkers are sorted regarding their number of linking positions: L_2: Dichloromethane (DCM), Dichloroethane (DCE), Dichloropropane (DCP), Dichlorobutane (DCB), and Bis(chloromethyl)benzene (BCMB); L_3: Chloroform ($CHCl_3$) and Tris(bromomethyl)benzene (TBMB); L_4: Tetrachloromethane (CCl_4) and Tetrakis(bromomethyl)benzene (TeBMB).

system and facilitate the sustainable and targeted generation of POPs *via* ball milling for the scientific community.

Results and discussion

The Polymer Matrix was developed through mechanochemical Friedel–Crafts polymerization, a reaction that involves a Lewis acid-catalysed C–C coupling between an aromatic monomer and a halide-containing linker in a high-speed ball mill (Fig. 1). To systematically investigate the impact of the molecular design on the formation of porous polymers, 16 aryl-containing monomers and 9 halide-containing linkers were selected for variation, each featuring unique structural characteristics. Despite the non-directed nature of the Friedel–Crafts polymerization, the molecular building blocks were sorted according to their symmetric unit to align with the classical covalent organic framework (COF) literature.[49,50] The monomers were grouped into C_2 (Naphthalene (NT), Anthracene (AT), Tetracene (TT), Biphenyl (BP), *p*-Terphenyl (TP), *p*-Quaterphenyl (QP), Tetraphenylethylene (TePE), and Tetraphenylbutadiene (TePB)), into C_3 (Triphenylamine (TPA), Triphenyltriazine (TPT), Triphenylbenzene (TPB), and Tris(*p*-biphenyl)benzene (TBB)), into T_d (Triphenylmethane (TPM) and Tetraphenylmethane (TePM)), and into C_6 (Benzene (BZ) and Hexaphenylbenzene (HPB)) symmetries (Fig. 1). It should be noted that the T_d category is not strictly applying to the point group, but to a tetrahedral structure of the respective building block. The linkers were categorized according to the number of linking points with L_2 (Dichloromethane (DCM), Dichloroethane (DCE), Dichloropropane (DCP), Dichlorobutane (DCB), and Bis(chloromethyl)benzene (BCMB)), L_3 (Chloroform ($CHCl_3$), and Tris(bromomethyl)benzene (TBMB)), and L_4 (Tetrachloromethane (CCl_4), and Tetrakis(bromomethyl)benzene (TeBMB)) linkers (Fig. 1).

In accordance to an established synthesis protocol, 1.63 mmol (1 eq.) monomer and 9.79 mmol (6 eq.) liquid linker or 1.63 mmol (1 eq.) solid linker were polymerized in the

presence of 5.22 g (39.16 mmol, 24 eq.) $AlCl_3$, simultaneously serving as Lewis acid and as bulk material.[44] The exact weights used for each monomer and linker can be found in Table S1 in the ESI.† All experiments were performed at 30 Hz for 1 h in 50 ml ZrO_2 vessels equipped with 22 ZrO_2 milling balls. After thorough milling, the resulting polymers were rinsed with water and acetone, and then dried at 80 °C over night.

The Polymer Matrix is comprised of 144 polymers, each produced with a specific combination of monomer and linker, and characterized by their respective yields, specific surface areas (SSA_{BET}), and total pore volumes at $P/P_0 = 0.95$. Tables S2–S9 in the ESI† provide the detailed information on each polymer, while Fig. S1–S34 (ESI†) graphically display the data of the tables, and the corresponding N_2 isotherms. In addition to this, Fig. S35 and S36 (ESI†) display the pore size distributions for polymers featuring total pore volumes of >0.5 cm^3 g^{-1}, revealing two main pore widths of 0.85 nm and 1.68 nm. The respective polymers comprise of smaller particles agglomerating to larger ones, while the contamination of Cl, Al and Zr was found to be <1 at%, respectively (see Fig. S37–S44 and Table S10–S13, ESI†). In general, the polymer yields vary from 0–99%, while some even exceed 100% as the starting materials are firmly embedded in the pores of the polymer and can no longer be removed from the product. Furthermore, the specific surface areas range from non-porous to 1300 m^2 g^{-1}. Although the specific surface areas are therefore smaller than those of comparable solution-based polymers, which in some cases even feature specific surface areas of up to 2500 m^2 g^{-1}, still highly porous materials are generated while simultaneously the green metrices and the synthesis time are improved by far.[51,52] In order to rationalize the results for a targeted generation of POPs, we have identified five possible building block characteristics that could determine reactivity and porosity, namely physical state and molecular size, geometry and flexibility, and electronic structure. To facilitate a deep understanding of the underlying principles, all characteristics are first examined with respect to their importance for the monomer, followed by the significance for the linker in the subsequent chapters.

Physical state and molecular size

The mechanochemical Friedel–Crafts reaction is carried out with an excess of $AlCl_3$, which simultaneously serves as catalyst and as bulk material to achieve a sufficient filling degree of the milling vessel. Even though the vessel is thus mainly loaded with solid material, the physical state, accompanied by the molecular size of the building blocks, proved to be an important parameter for the formation of porous polymers. In the following, the physical state and the molecular size of the monomers are examined, which is subsequently investigated for the linkers as well.

While the solid aromatic monomers HPB, TePE, and TBB readily form porous polymers with several linkers (see Fig. 2I), most polymers synthesized using the liquid monomer BZ exhibit low yields and small specific surface areas (see Fig. S29, ESI†). However, it is unlikely that the physical state of the monomer is solely responsible for the formation of porous polymers, as the use of other solid monomers such as

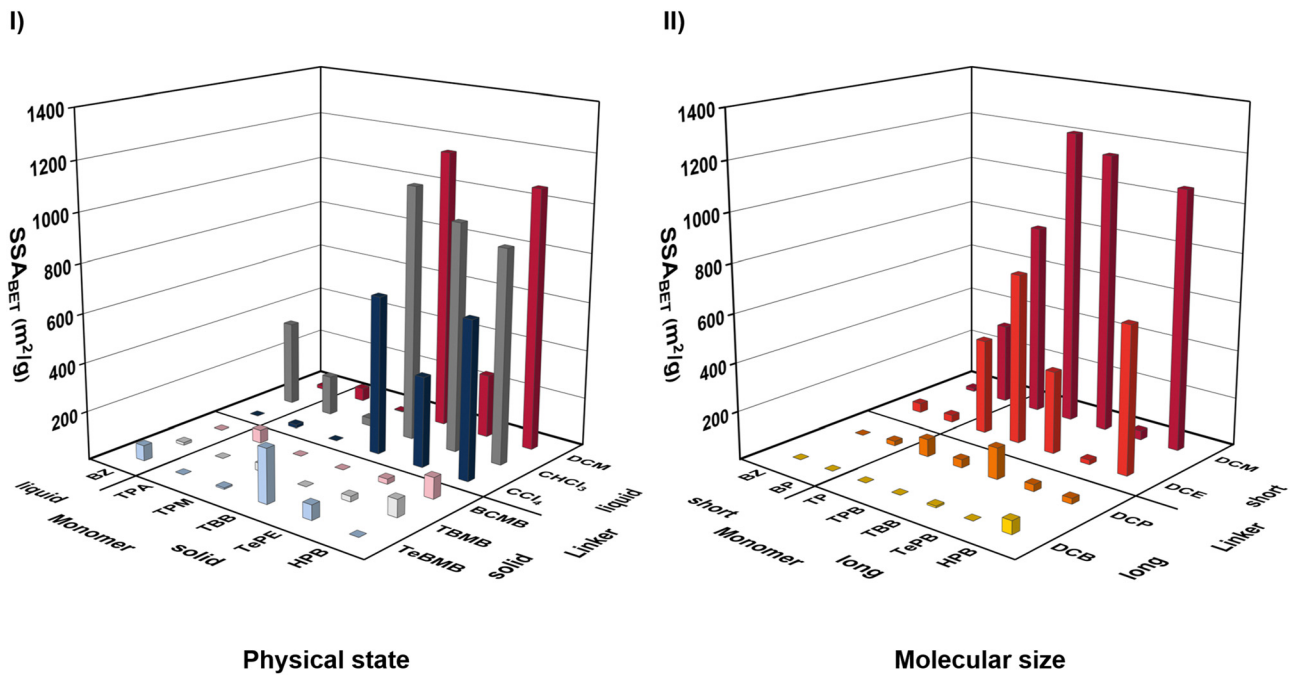

Fig. 2 (I) Overview over specific surface areas of porous polymers obtained for the polymerization of liquid (BZ) or solid (TPA, TPM, TBB, TePE, HPB) monomers with liquid (DCM (dark red), $CHCl_3$ (dark gray), CCl_4 (dark blue)) or solid (BCMB (pink), TBMB (light gray), TeBMB (light blue)) linkers. (II) Overview over specific surface areas of porous polymers obtained for the polymerization of shorter (BZ, BP) or longer (TP, TPB, TBB, TePB, HPB) monomers with shorter (DCM (dark red), DCE (light red)) or longer (DCP (orange), DCB (yellow)) linkers.

TPM or TPA also results in the generation of polymers with reduced yields and specific surface areas (Fig. 2I).

Since the physical state is in direct correlation with the molecular length, the inadequate performance of BZ can be attributed to its small size, which is diminishing the amount of possible resonance-stabilization (see chapter on Electronic structure). An increase in monomer length towards BP or TP not only results in higher yields, but also in an enhancement of the respective porosities (Fig. 2II). In general, a larger size of the monomer is advantageous for a higher porosity of the polymer, as it can be seen in the example of **HPB–DCM**, **TBB–DCM** and **TPB–DCM**, all of which feature specific surface areas of $>1000\ m^2\ g^{-1}$ (Fig. 2II). However, caution must be taken when using monomers with elongated alkene chains, such as TePB, as the linker may attack the center of the monomer, resulting in a decline in specific surface area due to pore penetration (Fig. 2II and Fig. S15, ESI†).

Opposing the monomer characteristics, the physical state of the linker is of high significance for the Friedel–Crafts polymerization. In contrast to liquid linkers, solid ones either feature an aryl moiety or comprise of an elongated alkyl chain. In the first case, the obtained polymers feature significantly lower SSA_{BET} compared to the polymers generated by applying their liquid analogues (see Table S2–S8 and Fig. 2I, ESI†). For example, replacing the bidentate solid linker BCMB with the bidentate liquid linker DCM prompts an enhancement of the specific surface area from non-porous to 1153 $m^2\ g^{-1}$ for the polymerization of TBB. A similar trend can be observed for the tridentate linkers TBMB (solid) and $CHCl_3$ (liquid) (see Fig. 2I). Although the reaction rheology is a very important parameter of a mechanochemical polymerization, as already demonstrated on several occasions, even a heating of the milling vessel to change the physical state of the solid linkers would probably not result in higher porosities the respective polymers.[42,45,48] The reason for this is the possibility of simultaneous self-polymerization of the aryl-containing solid linker. In the classical Friedel–Crafts polymerization, the coordination of the Lewis acid and the halide-atom of the linker induces the formation of a positive polarization on the adjacent carbon of the linker, which is subsequently attacked by the high electron density of the monomer to form a polymer under rearomatisation (Fig. 1). By using a solid aryl-containing linker, the high electron density of a second linker molecule can fulfil the monomer part, which is not feasible for a liquid linker without aryl moiety (Fig. S45, ESI†). Consequently, the solid aryl-containing linker reacts with itself and traps the monomer molecules in the pores of the polymer, causing low specific surface areas and high yields. Nevertheless, this self-polymerization can prevail the formation of porous polymers with specific surface areas of up to 700 $m^2\ g^{-1}$ (SP-TBMB) when no monomer is added to the reaction mixture (Fig. S33 and Table S9, ESI†).

In the second case, linkers featuring elongated alkyl-chains could also be implemented as solid analogues. To investigate the impact of the linker size on the formation of a porous polymer, DCM was substituted with DCE, DCP and DCB. Independent on the choice of the monomer, a longer linker causes a decrease in polymer porosity (Fig. 2II). Additionally, DCB generates polymers in very low yields in most cases. During the reaction, the halide bonded to the aliphatic linker enhances the positive polarization of the carbon atom of the linker. Increasing the aliphatic chain length and thus the distance between the point of attack and the second halide atom, leads to a mediocre polarization and therefore to lower degrees of polymerization.

The results are remarkable, as the building block requirements for the generation of porous polymers are very different with respect to monomers and linkers. While the physical state plays no role for the monomers, it is very important for the linkers. Additionally, a larger size of the monomer is advantageous, while contrary to this a small linker is most suitable for the formation of porous polymers. Based on the results, we focus on the use of small liquid linkers, such as DCM, $CHCl_3$ and CCl_4, in the subsequent chapters.

Geometry and flexibility

Besides the physical state and size of the building blocks, their geometry and flexibility are important characteristics for the formation of porous polymers as well. Again, these characteristics are first examined for the monomer, followed by the linker in the subsequent paragraph.

To investigate the influence of the monomer geometry in more detail, TP (C_2), TePE (C_2), TPB (C_3), TePM (T_d) and HPB (C_6) were selected as representative examples for their respective categories to minimize the impact of different sizes and electronic structures on the investigation of the polymer formation (Fig. S46, ESI†). Except from TePM, all other monomers prevailed the formation of porous polymers featuring high specific surface areas when combined with DCM, $CHCl_3$ or CCl_4 as linker (Fig. 3I). The tetrahedral structure of TePM, with a central sp^3 hybridized carbon, should ideally form three-dimensional networks, but the non-directional nature of the Friedel–Crafts reaction, combined with this geometry, results in a dense packing of the monomers in the polymer and probably leads to pore penetration through the phenyl rings.[45] Furthermore, the narrow packing could cause inaccessibility of the pores for the adsorption of nitrogen during the physisorption measurement. In contrast, trigonal or hexagonal monomers (TPB and HPB) are more suitable for generating highly porous polymers (see Fig. 3I). Despite the 62° twist of the phenyl rings in HPB against the central ring, the nearly planar geometry of these monomers, in combination with structurally directing linkers, induces the formation of polymers with easily accessible pores.[53]

Although the C_2 monomer TePE features a similar strained architecture as HPB with the four phenyl rings tilted at 50° against the central olefin bond in an unique propeller shape, the formation of polymers with smaller specific surface areas predominates when polymerizing this monomer compared to HPB (see Table S4 and S8, ESI†).[54] The reason for this is a highly rigid arrangement of the monomer due to the strong steric hinderance of the phenyl rings, as the central double

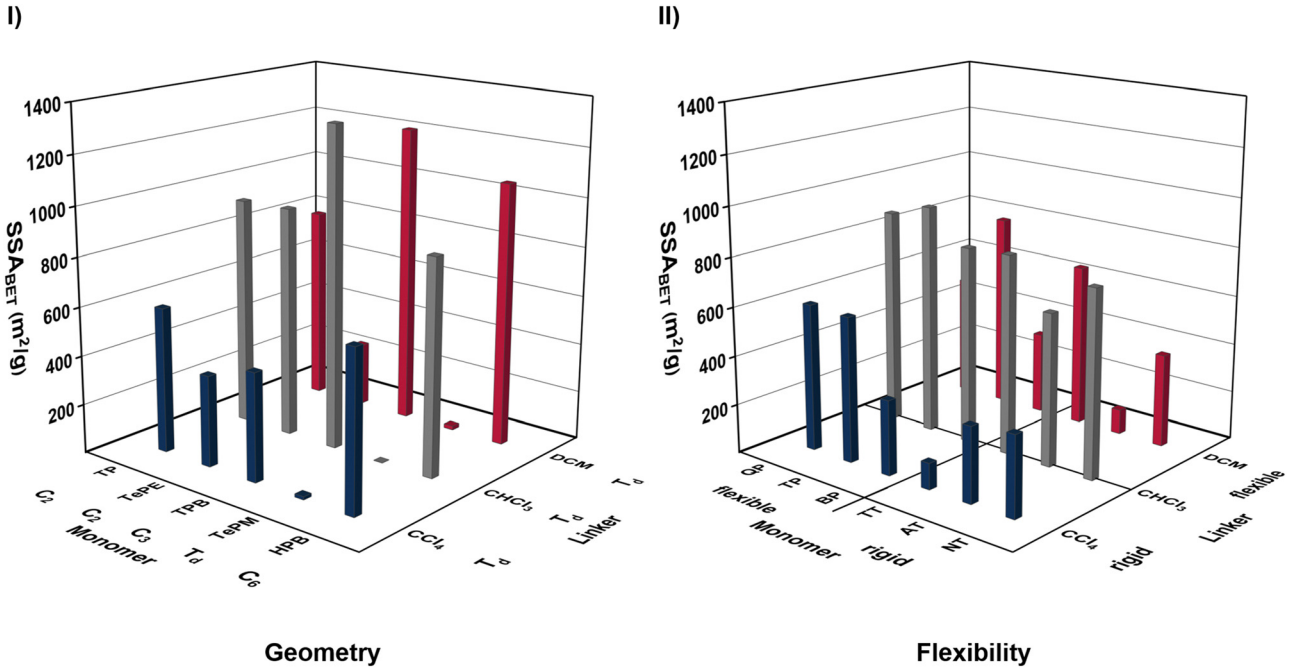

Fig. 3 (I) Overview over specific surface areas of porous polymers obtained for the polymerization of C_2 monomers (TP, TePE), of a C_3 monomer (TPB), of a T_d monomer (TePM) and of a C_6 monomer (HPB) with the T_d linkers DCM (dark red), $CHCl_3$ (dark gray) and CCl_4 (dark blue). (II) Overview over specific surface areas of porous polymers obtained for the polymerization of flexible (QP, TP, BP) or rigid (TT, AT, NT) monomers with the increasingly rigid linkers DCM (dark red), $CHCl_3$ (dark gray) and CCl_4 (dark blue).

bond and the phenyl rings are not coplanar. The use of a more flexible C_2 monomer, such as TP, leads to an increase of the porosity (see **TP–DCM** with 796 m^2 g^{-1} and **TePE–DCM** with 261 m^2 g^{-1}), nevertheless in general a linear monomer geometry is slightly less efficient for the formation of porous polymers than a trigonal or hexagonal planar one (see Fig. 3I).

To investigate the impact of the monomer flexibility in more detail, the isolated-ring monomer TP and its structurally similar monomers BP and QP were compared to their fused-ring analogues AT, NT, and TT. The isolated-ring monomers have the ability to rotate freely around the C–C′ bond, whereas the fused-ring systems are planar and rigid. Although for smaller monomers, such as BP and NT, a very similar polymerization behavior of flexible and rigid monomers was observed, the substitution towards TP and AT or towards QP and TT led to varying porosities of the respective polymers (see Fig. 3II). Apparently, the higher flexibility of the isolated-ring monomers TP and QP results in the formation of polymers with slightly increased specific surface areas (*e.g.* **TP–CCl_4** with 592 m^2 g^{-1} *vs.* **AT–CCl_4** with 306 m^2 g^{-1} and **QP–CCl_4** with 600 m^2 g^{-1} *vs.* **TT–CCl_4** with 107 m^2 g^{-1}). Nevertheless, this might be attributed to the respective substitution pattern, as the fused-ring monomers AT and TT are preferably linked at the carbon atoms of the central rings. Thereby, the outer rings of the monomers penetrate the pores of the polymers, which is diminishing the porosity.

In contrast to the monomer, the geometry of the linker was found to be a subordinate building block characteristic in the Friedel–Crafts polymerization. Although the linkers DCM, $CHCl_3$ and CCl_4 all exhibit a tetrahedral structure with an angle of approximately 109.5° between the chlorine atoms, they behave vastly different in the mechanochemical Friedel–Crafts reaction. For instance, the polymerization of TPB with DCM facilitates the formation of a polymer with a specific surface area of 1220 m^2 g^{-1} (**TPB–DCM**), while the exchange towards CCl_4 causes the formation of a polymer with a SSA_{BET} of 440 m^2 g^{-1} (**TPB–CCl_4**) (see Fig. 3I). In direct comparison, the application of DCM leads to higher specific surface areas of the polymers synthesized with 12 of the 16 monomers, while the use of CCl_4 results in higher yields in most cases (see Table S2–S8, ESI†).

The observed difference in behavior is attributed the number of linking positions of the two linkers and thereby to the flexibility of the formed polymers. DCM has only two linking positions, resulting in very flexible porous structures that are susceptible to changes in milling parameters.[44] In contrast, CCl_4 is exhibiting four linking positions, leading to the formation of highly rigid networks that can trap residuals of the monomer or Lewis acid in the pores, resulting in high yields but reduced specific surface areas. The use of $CHCl_3$ as a threefold linker combines both factors, prevailing the formation of rigid polymers that are insensitive to parameter changes but not too rigid. Thus, a L_3 linker arrangement was found to be most promising for the formation of porous polymers in very high yields and with excellent specific surface areas (see Table S2–S8, ESI†).

Again, the chapter emphasizes the different requirements of the building blocks for the formation of porous polymers.

While the monomer geometry is very important for the porosity of a polymer, this characteristic plays a subordinate role for the linker. Conversely, the flexibility of the monomer in this reaction is by far not as significant as it is for the linker.

Electronic structure

The electronic structure of the building blocks is crucial for the formation of porous polymers as well, as it will be examined for monomers and linkers, respectively, in the following.

For instance, replacing highly conjugated monomers such as TPB with monomers with reduced conjugation between the phenyl rings (TPM or TePM) drastically diminishes the yields and the specific surface areas of the respective polymers (see Table S7, ESI†). This is because the reduced conjugation results in a decrease in resonance stabilization in the Friedel–Crafts polymerization. During this reaction, the coordination of the Lewis acid and the linker is followed by a nucleophilic attack of the electron-rich monomer at the positively polarized carbon atom of the linker, leading to the formation of a transition state (Fig. 4). By the release of $AlCl_4^-$, the carbenium ion intermediate is formed, which is stabilized by the delocalization of the positive charge. A highly conjugated monomer is capable to stabilize this carbenium ion more effectively than a monomer exhibiting a reduced conjugation. To investigate this further, quantum chemical calculations were carried out to determine the energy input required for the first step of the Friedel–Crafts polymerization reaction and thus for the likelihood of the reaction to proceed. Therefore, the starting materials, the transition state and the intermediate were calculated by means of B3LYP/6-311+G*. For the polymerization of DCM and BZ, the Gibbs free energy value of the transition state was calculated to be 24.55 kcal mol^{-1} (Fig. 4). As this value is quite high, the respective polymer **BZ–DCM** was obtained in a mediocre yield of 23%. In contrast, substituting BZ with the highly conjugated TPB facilitates the formation of a polymer with a yield of 95%. Accompanying this, the transition state of BP (model compound of TPB) was calculated to exhibit a drastically reduced ΔG value of 21.53 kcal mol^{-1} (Fig. 4). The substitution of the central ring in TPB with triazine, such as it is the case for structurally analogue TPT, leads to a reduction in yield for the polymerization with DCM, dropping to 55% (see Fig. S19 and S21, ESI†). This is due to the nitrogen entities in the triazine core that hinder the delocalization of charge involving the central ring, resulting in a reduced amount of resonance structures (see Fig. S47, ESI†). Due to this, the calculated transition state of DCM and Phenyltriazine (PT; model compound for TPT) was found to exhibit a very high ΔG value of 26.70 kcal mol^{-1}. This indicates that the reaction between TPB and DCM proceeds much more readily than between TPT and DCM.

For the linker, the number of halides bonded to the linking carbon atom is an important factor for the reaction process. When comparing the polymerization of the model compound BP for TPB with $CHCl_3$ and with CCl_4, similar Gibbs free energy values

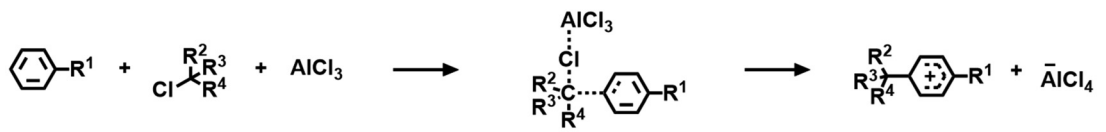

Monomer	Linker	ΔG (kcal/mol)	ΔE (kcal/mol)	ΔG (kcal/mol)	ΔE (kcal/mol)
BZ	DCM	24.55	21.16	10.20	5.16
	$CHCl_3$	24.29	20.61	8.20	3.30
	CCl_4	24.76	18.19	5.34	-2.34
BP (MC of TPB)	DCM	21.53	18.37	0.92	-4.18
	$CHCl_3$	19.52	16.32	-1.21	-8.04
	CCl_4	19.91	14.29	-6.72	-13.23
PT (MC of TPT)	DCM	26.70	22.79	11.21	5.05
	$CHCl_3$	26.10	21.78	8.52	1.12
	CCl_4	27.35	21.18	11.40	3.87

Fig. 4 Top: Schematic overview over the formation of the transition state and of the intermediate during the first reaction step of the mechanochemical Friedel–Crafts polymerization. Bottom: Gibbs free energy (ΔG) and total energy (ΔE) values, in kcal mol^{-1}, of the transition state and of the intermediate for the polymerization of monomers and linkers calculated by means of B3LYP/6-311+G*. For the calculation the monomers BZ (top), BP (middle; model compound for TPB) and PT (bottom; model compound of TPT), and the linkers DCM, $CHCl_3$ and CCl_4 were used.

Table 1 Classification of the building block characteristics in terms of their importance and the requirements for monomers and linkers with regard to the formation of porous polymers

	Monomer		Linker	
	Importance	Requirement	Importance	Requirement
Physical state	Not important	—	Important	Liquid
Molecular length	Important	Long	Important	Short
Geometry	Important	C_3/C_6	Not important	—
Flexibility	Not important	—	Important	L_3
Electronic structure	Important	High delocalization	Important	High polarization

for the respective transition states were observed (ΔG **BP–CHCl$_3$** = 19.52 kcal mol^{-1} and ΔG **BP–CCl$_4$** =19.91 kcal mol^{-1}). However, the total energy (ΔE) required for the use of CCl_4 as linker is smaller, indicating that the formation of the transition state requires a lower energy input during the polymerization with CCl_4, although the reactions are equally likely to proceed. This is due to the additional chlorine bonded to the linker, which can withdraw more electrons from the linking carbon in the starting material and thus facilitate the attack of the aromatic monomer. Furthermore, the number of halides bonded to the linking carbon atom affects the Gibbs free energy value of the intermediate. While the polymerization of BP with DCM results in the formation of an intermediate with a ΔG value of 0.92 kcal mol^{-1}, the use of $CHCl_3$ or CCl_4 causes an increased stabilization of the intermediate. As the corresponding Gibbs free energy values are negative with −1.21 kcal mol^{-1} and −6.72 kcal mol^{-1} for the use of $CHCl_3$ and CCl_4, respectively, these intermediates even feature a higher stability than the starting materials. Consequently, the polymerization is accomplished in higher yields than for the use of DCM (Table S6, ESI†). However, it should be noted that a higher amount of chlorine bonded to the linker also leads to a reduced flexibility of the polymer, which in turn diminishes its porosity, as discussed in the previous chapter.

As the electronic structure of the building blocks is substantially responsible for the formation of the polymer in the first case, this characteristic was found to be most important with respect to the yield, while the aforementioned characteristics are more essential for designing the porosity of the respective polymers.

Classification

It is important to note that the characteristics examined in this investigation are often mutually dependent and interconnected. The requirements for monomers and linkers to achieve the formation of porous polymers cannot be considered in isolation. While we have attempted to evaluate the importance of individual properties of the building blocks in terms of yield and specific surface area by comparing structurally different monomers and linkers, it is essential to consider these characteristics in the overall context of polymer design. The interplay of various factors such as electronic structure, steric hindrance, linker functionality, and halogen-content ultimately determines the properties of the resulting porous polymer.

Table 1 provides a comprehensive overview of the key characteristics of building blocks and their respective requirements for the formation of porous polymers *via* mechanochemistry. As depicted in the table, the design of the monomer plays a critical role in the generation of porous polymers, with a long and highly delocalized C_3 or C_6 geometry being ideal for achieving high specific surface areas and yields. For the linker, a short and liquid structure with an L_3 linking arrangement and a high polarization of the linking carbon is essential for optimum porosity. These design principles are crucial for the prediction of the porosity of a desired polymer in a mechanochemical polymerization, and will hopefully encourage more researchers to explore the potential of solvent-free POPs synthesis as a sustainable alternative in the future.

Conclusion

Herein, we have presented a comprehensive investigation into the origin of porosity in a mechanochemical Friedel–Crafts reaction by developing a Polymer Matrix tool. By polymerizing 16 aromatic monomers and 9 halide-containing linkers in a high-speed ball mill, we generated 144 polymers and identified the critical characteristics required for the formation of highly porous polymers. We found that the physical state, molecular size, geometry and flexibility, and electronic structure of the building blocks play crucial roles in determining the porosity of the resulting polymers. Specifically, the monomer must exhibit a large size, a trigonal or hexagonal planar geometry, and strong delocalization of the π-system to generate highly porous polymers in high yields. The linker should be small and liquid, with a tridentate linking arrangement to maintain an appropriate balance between stability and rigidity of the polymer. Our findings underscore the stark differences in requirements between monomers and linkers for the formation of porous polymers, and highlight the importance of considering each characteristic in the overall context. Such important building instructions could only be discovered through an extensive Polymer Matrix and will aid researchers in the targeted design of porous polymers. This will hopefully promote the solvent-free generation of such materials, which are for example applicable in catalysis or molecular separations, as a sustainable alternative in the future.

Experimental section

Mechanochemical polymer matrix

In a typical synthesis approach 1.63 mmol (1 eq.) monomer and 9.79 mmol (6 eq.) liquid linker or 1.63 mmol (1 eq.) solid linker,

respectively, were polymerized in the presence of 5.22 g (39.16 mmol, 24 eq.) $AlCl_3$, serving as Lewis acid and as bulking material. The used weights for each monomer and linker are presented in Table S1 in the ESI.† Based on an established mechanochemical synthesis protocol, the reactions were proceeded in a 50 ml ZrO_2 milling jar with 22 ZrO_2 milling balls ($\varnothing$ = 10 mm, average weight 3.2 g) in a Retsch MM500 mixer mill.[44] Thereby, each reaction was milled for 1 hour at 30 Hz, followed by a subsequent workup with water and acetone. The synthesized polymers were dried at 80 °C overnight.

Analysis

Physisorption measurements were carried out on a Quantachrome Quadrasorb instrument at 77 K with high purity nitrogen gas (N_2 : 99.99%). Prior to the measurement, the samples were outgassed at 423 K for 24 h. The specific surface areas (SSA) of all polymers were calculated by using the BET (Brunauer, Emmett, Teller) equation, while the total pore volumes were estimated at the adsorption branch at P/P_0 = 0.95. Both values can be found for each polymer in Table S2–S9 in the ESI.† Pore size distributions for polymers featuring total pore volumes of >0.5 m^2 g^{-1} were obtained by DFT calculations applying the calculation model N_2 at 77 K on carbon (slit pore, QSDFT equilibrium model).

SEM images were recorded at a voltage of 3 kV with the high-resolution scanning electron microscope JEOL JSM-IT800SHL. For EDS an Oxford Ultim Max Silicon Drift Detector (SDD) was used as primary detector.

Calculation

For all calculations the B3LYP functional in combination with the 6-311+G* basis set was used.[55–58] Furthermore, the Gaussian 16 program package was used for all calculations.[59] In order to minimize the computational cost, BP was chosen as the model compound for TPB and PT for TPT. The model compounds were chosen as they involve both the linker's point of attack on the outer ring and the central ring of the represented monomer. All calculations were accomplished for the use of DCM, $CHCl_3$ and CCl_4 as linkers.

Author contributions

Annika Krusenbaum: conceptualization, data curation, formal analysis, investigation, methodology, verification, visualization, writing – original draft. Steffi Krause Hinojosa: formal analysis, investigation, verification. Sven Fabig: formal analysis, methodology, verification. Valentin Becker: formal analysis, investigation, verification. Sven Grätz: conceptualization, data curation, funding acquisition, project administration, resources, supervision, writing – review & editing. Lars Borchardt: conceptualization, data curation, funding acquisition, project administration, resources, supervision, writing – review & editing.

Conflicts of interest

There are no conflicts to declare.

Acknowledgements

The authors gratefully acknowledge the Federal Ministry of Education and Research (Bundesministerium für Bildung und Forschung, BMBF) for support of the Mechanocarb project (award number 03SF0498) and the German Research Foundation (Deutsche Forschungsgemeinschaft, DFG) for funding the project 469290370. Furthermore, the authors express their gratitude to Stefanie Hutsch for SEM and EDS recordings.

References

1 J.-X. Jiang, F. Su, A. Trewin, C. D. Wood, N. L. Campbell, H. Niu, C. Dickinson, A. Y. Ganin, M. J. Rosseinsky, Y. Z. Khimyak and A. I. Cooper, *Angew. Chem., Int. Ed.*, 2007, **46**(45), 8574.
2 S. Kitagawa, R. Kitaura and S. Noro, *Angew. Chem., Int. Ed.*, 2004, **43**(18), 2334.
3 N. B. McKeown and P. M. Budd, *Chem. Soc. Rev.*, 2006, **35**(8), 675.
4 C. Özen, K. Obata, P. Bogdanoff, N. Yulianto, H. S. Wasisto and F. F. Abdi, *Sustainable Energy Fuels*, 2022, **6**(2), 377.
5 Q. Pujol, G. Weber, J.-P. Bellat, S. Grätz, A. Krusenbaum, L. Borchardt and I. Bezverkhyy, *Microporous Mesoporous Mater.*, 2022, **344**, 112204.
6 W. Lu, D. Yuan, D. Zhao, C. I. Schilling, O. Plietzsch, T. Muller, S. Bräse, J. Guenther, J. Blümel, R. Krishna, Z. Li and H.-C. Zhou, *Chem. Mater.*, 2010, **22**(21), 5964.
7 D. Taylor, S. J. Dalgarno, Z. Xu and F. Vilela, *Chem. Soc. Rev.*, 2020, **49**(12), 3981.
8 K. Cousins and R. Zhang, *Polymers*, 2019, **11**(4), 690.
9 A. Li, R.-F. Lu, Y. Wang, X. Wang, K.-L. Han and W.-Q. Deng, *Angew. Chem., Int. Ed.*, 2010, **49**(19), 3330.
10 P. Bhanja, S. K. Das, K. Bhunia, D. Pradhan, T. Hayashi, Y. Hijikata, S. Irle and A. Bhaumik, *ACS Sustainable Chem. Eng.*, 2018, **6**(1), 202.
11 P. Xiao and Y. Xu, *J. Mater. Chem. A*, 2018, **6**(44), 21676.
12 F. Vilela, K. Zhang and M. Antonietti, *Energy Environ. Sci.*, 2012, **5**(7), 7819.
13 Q. Sun, Z. Dai, X. Meng and F.-S. Xiao, *Chem. Soc. Rev.*, 2015, **44**(17), 6018.
14 S. Kim, B. Kim, N. A. Dogan and C. T. Yavuz, *ACS Sustainable Chem. Eng.*, 2019, **7**(12), 10865.
15 K. Dong, Q. Sun, X. Meng and F.-S. Xiao, *Catal. Sci. Technol.*, 2017, **7**(5), 1028.
16 Z. Li and Y.-W. Yang, *Adv. Mater.*, 2022, **34**(6), e2107401.
17 X. Liu, C.-F. Liu, W.-Y. Lai and W. Huang, *Adv. Mater. Technol.*, 2020, 2000154.
18 G. Ji, Y. Zhao and Z. Liu, *Green Chem. Eng.*, 2022, **3**(2), 96.
19 H. L. Nguyen, N. Hanikel, S. J. Lyle, C. Zhu, D. M. Proserpio and O. M. Yaghi, *J. Am. Chem. Soc.*, 2020, **142**(5), 2218.

20 F. M. Wisser, K. Eckhardt, D. Wisser, W. Böhlmann, J. Grothe, E. Brunner and S. Kaskel, *Macromolecules*, 2014, **47**(13), 4210.
21 P. Kaur, J. T. Hupp and S. T. Nguyen, *ACS Catal.*, 2011, **1**(7), 819.
22 D.-H. Yang, Y. Tao, X. Ding and B.-H. Han, *Chem. Soc. Rev.*, 2022, **51**(2), 761.
23 Y. Zhao, Y. He and T. M. Swager, *ACS Macro Lett.*, 2018, **7**(3), 300.
24 H. Zhong, G. Wu, Z. Fu, H. Lv, G. Xu and R. Wang, *Adv. Mater.*, 2020, **32**(21), e2000730.
25 M. S. Lohse and T. Bein, *Adv. Funct. Mater.*, 2018, **28**(33), 1705553.
26 X.-J. Zhang, N. Bian, L.-J. Mao, Q. Chen, L. Fang, A.-D. Qi and B.-H. Han, *Macromol. Chem. Phys.*, 2012, **213**(15), 1575.
27 D. Zhou, X. Tan, H. Wu, L. Tian and M. Li, *Angew. Chem.*, 2019, **131**(5), 1390.
28 L. Tan and B. Tan, *Chem. Soc. Rev.*, 2017, **46**(11), 3322.
29 R. A. Sheldon, *Green Chem.*, 2017, **19**(1), 18.
30 C. S. Slater, M. J. Savelski, W. A. Carole and D. J. C. Constable, in Green chemistry in the pharmaceutical industry. Green chemistry, *Solvent Use and Waste Issues*, ed. Dunn P. J., Wells A. S., Williams M. T., Williams M. T., Dunn P. J., Wiley-VCH, Weinheim, 2010. pp. 49–82.
31 *Mechanochemistry*, ed. Colacino E., Ennas G., Halasz I., Porcheddu A., Scano A., De Gruyter, 2020.
32 A. Krusenbaum, S. Grätz, G. T. Tigineh, L. Borchardt and J. G. Kim, *Chem. Soc. Rev.*, 2022, **51**(7), 2873.
33 J.-L. Do and T. Friščić, *ACS Cent. Sci.*, 2017, **3**(1), 13.
34 T. Friščić, C. Mottillo and H. M. Titi, *Angew. Chem., Int. Ed.*, 2020, **59**(3), 1018.
35 E. Boldyreva, *Chem. Soc. Rev.*, 2013, **42**(18), 7719.
36 J. L. Howard, Q. Cao and D. L. Browne, *Chem. Sci.*, 2018, **9**(12), 3080.
37 D. Tan, L. Loots and T. Friščić, *Chem. Commun.*, 2016, **52**(50), 7760.
38 T. Rensch, S. Fabig, S. Grätz and L. Borchardt, *ChemSusChem*, 2022, **15**(1), e202101975.
39 S. Karak, S. Kandambeth, B. P. Biswal, H. S. Sasmal, S. Kumar, P. Pachfule and R. Banerjee, *J. Am. Chem. Soc.*, 2017, **139**(5), 1856.
40 K. Jie, Y. Zhou, Q. Sun, B. Li, R. Zhao, D. Jiang, W. Guo, H. Chen, Z. Yang, F. Huang and S. Dai, *Nat. Commun.*, 2020, **11**(1), 1086.
41 S. Grätz, B. Wolfrum and L. Borchardt, *Green Chem.*, 2017, **19**(13), 2973.
42 A. Krusenbaum, S. Grätz, S. Bimmermann, S. Hutsch and L. Borchardt, *RSC Adv.*, 2020, **10**(43), 25509.
43 S. Grätz, M. Oltermann, E. Troschke, S. Paasch, S. Krause, E. Brunner and L. Borchardt, *J. Mater. Chem. A*, 2018, **6**(44), 21901.
44 A. Krusenbaum, J. Geisler, F. J. L. Kraus, S. Grätz, M. V. Höfler, T. Gutmann and L. Borchardt, *J. Polym. Sci.*, 2022, **60**(1), 62.
45 J.-S. M. Lee, T. Kurihara and S. Horike, *Chem. Mater.*, 2020, **32**(18), 7694.
46 E. Troschke, S. Grätz, T. Lübken and L. Borchardt, *Angew. Chem., Int. Ed.*, 2017, **56**(24), 6859.
47 A. Krusenbaum, F. J. L. Kraus, S. Hutsch, S. Grätz, M. V. Höfler, T. Gutmann and L. Borchardt, *Adv. Sustainable Syst.*, 2023, 2200477.
48 S. Grätz, S. Zink, H. Kraffczyk, M. Rose and L. Borchardt, *Beilstein J. Org. Chem.*, 2019, **15**, 1154.
49 N. Huang, P. Wang and D. Jiang, *Nat. Rev. Mater.*, 2016, **1**, 10.
50 A. Tyagi and S. Kolay, in Handbook on Synthesis Strategies for Advanced Materials, *Synthesis of Metal Organic Frameworks (MOF) and Covalent Organic Frameworks (COF)*, Springer, Singapore, 2021, pp. 503–556.
51 H. Zhou, C. Rayer, A. R. Antonangelo, N. Hawkins and M. Carta, *ACS Appl. Mater. Interfaces*, 2022, **14**(18), 20997.
52 K. J. Msayib and N. B. McKeown, *J. Mater. Chem. A*, 2016, **4**(26), 10110.
53 S. Dalapati, M. Addicoat, S. Jin, T. Sakurai, J. Gao, H. Xu, S. Irle, S. Seki and D. Jiang, *Nat. Commun.*, 2015, **6**, 7786.
54 M. Villa, P. Ceroni and A. Fermi, *ChemPlusChem*, 2022, **87**(4), e202100558.
55 A. D. Becke, *Phys. Rev. A Gen. Phys.*, 1988, **38**(6), 3098.
56 C. Lee, W. Yang and R. G. Parr, *Phys. Rev. B: Condens. Matter Mater. Phys.*, 1988, **37**(2), 785.
57 B. Miehlich, A. Savin, H. Stoll and H. Preuss, *Chem. Phys. Lett.*, 1989, **157**(3), 200.
58 T. Clark, J. Chandrasekhar, G. W. Spitznagel and P. V. R. Schleyer, *J. Comput. Chem.*, 1983, **4**, 294.
59 M. J. Frisch, G. W. Trucks, H. B. Schlegel, G. E. Scuseria, M. A. Robb, J. R. Cheeseman, G. Scalmani, V. Barone, G. A. Petersson, H. Nakatsuji, X. Li, M. Caricato, A. V. Marenich, J. Bloino, B. G. Janesko, R. Gomperts, B. Mennucci, H. P. Hratchian, J. V. Ortiz, A. F. Izmaylov, J. L. Sonnenberg Williams, F. Ding, F. Lipparini, F. Egidi, J. Goings, B. Peng, A. Petrone, T. Henderson, D. Ranasinghe, V. G. Zakrzewski, J. Gao, N. Rega, G. Zheng, W. Liang, M. Hada, M. Ehara, K. Toyota, R. Fukuda, J. Hasegawa, M. Ishida, T. Nakajima, Y. Honda, O. Kitao, H. Nakai, T. Vreven, K. Throssell, J. A. Montgomery Jr., J. E. Peralta, F. Ogliaro, M. J. Bearpark, J. J. Heyd, E. N. Brothers, K. N. Kudin, V. N. Staroverov, T. A. Keith, R. Kobayashi, J. Normand, K. Raghavachari, A. P. Rendell, J. C. Burant, S. S. Iyengar, J. Tomasi, M. Cossi, J. M. Millam, M. Klene, C. Adamo, R. Cammi, J. W. Ochterski, R. L. Martin, K. Morokuma, O. Farkas, J. B. Foresman and D. J. Fox, *Gaussian 16 Rev. C.01*, Wallingford, CT, 2016.